# Partition of unity methods for approximation of point water sources in porous media

Pavel Exner[a,*], Jan Březina[a]

[a] *Technical University of Liberec, Studentská 1402/2, 461 17 Liberec 1, Czech Republic*

**Abstract**

In this work we demonstrate usage of Partition of Unity (PU) methods to improve approximation of singularities in the solution of the Poisson equation. Our model describes a steady flow of water in a system of aquifers which consist of porous media. The aquifers are perforated by wells and boreholes which are often represented as point sources considering their small diameter in comparison with the vast size of the aquifer. This brings singularities into the solution. The extended and stable generalized finite element method (XFEM and SGFEM) were implemented to solve the problem and a proper adaptive integration strategy was developed to gain optimal convergence rates.

*Keywords:* PUM, XFEM, SGFEM, adaptive integration, point sources

## 1. Introduction

People often consider in their models of flow in porous media very large areas which can contain various phenomena of very small scale compared with the size of the areas. These can be some disruptions of the porous media, e.g. cracks and wells, or material inhomogeneities that cause large gradients in pressure head and velocity or even their discontinuities.

Using the standard finite element method (FEM) we are unable to properly approximate the quantities in the vicinity of these disturbances, unless

*Corresponding author.

*Email addresses:* pavel.exner@tul.cz (Pavel Exner), jan.brezina@tul.cz (Jan Březina)

*URL:* https://github.com/Paulie14/xfem_project (Pavel Exner)

we introduce elements of the same scale in the mesh. This leads to higher requirements on mesh processing (refinement) and increase of computational costs due to growing number of degrees of freedom.

In this work we use PU (Partition of Unity) methods to overcome these problems and demonstrate it on a steady two-dimensional aquifer model containing hydro-geological wells which cause singularities in solution. We follow the work [1, 2] of Gracie and Craig who have already used the XFEM (eXtended FEM) on a similar model. However, we focus mainly on the study of the PU methods. In particular, we use the XFEM and its corrected version (including ramp function and shift), e.g. by Fries in [3], and the SGFEM introduced by Babuška and Banerjee in [4, 5]. We measure the convergence of pressure head in $L^2$ norm over the aquifer domain and we compare the used methods. We also investigate the error of the adaptive integration on the enriched elements and introduce improvement. In addition, we suggest better choice of enrichment area based on a tolerance criterion.

The implementation was done in C++ language using the Deal II library [6], the finite element library. which does not support any enrichment techniques at the moment.

We describe the model in the beginning of the article, set the problem and go through the PU methods in more details. Then we show some numerical aspects of the problem which we must deal with, especially the adaptive integration in section 5. Results, convergence of methods and conditioning of the algebraic system are discussed right after and further research goals are pointed out at the end.

## 2. Model

We consider a steady flow in a system of aquifers (2D horizontal layers of given thickness) which are separated by impermeable layers (aquitards). The aquifers are connected by wells which act as sources or sinks in the domain of each aquifer. The pressure in the aquifers is further governed by the boundary condition of the aquifers which can be of Dirichlet type or be homogeneous of Neumann type.

We describe the wells as interior boundary condition therefore we need to define the computational domain as the aquifer domain with wells cross-sections cut off. Let the $\Theta^m$ be the domain on $m$-th aquifer, $m = 1, \dots M$, and $z_m$ be the vertical coordinate of the aquifer. The well $w$ is defined by a cylinder $B_w$ with the base center $\boldsymbol{x}_w$, radius $r_w$ and height $|z_1 - z_M|$. We

further denote $B_w^m = B_W \cap \Theta^m$ the cross-section of the aquifer $m$ and the well $w \in \mathcal{W} = \{1, \ldots, W\}$ and the union $B^m = \bigcup_w B_w^m$. We can then define domain $\Omega^m = \Theta^m \setminus B^m$ with an exterior boundary consisting of exclusive parts $\partial\Theta^m = \Gamma_D^m \cup \Gamma_N^m$ and an interior boundary $\partial B^m = \bigcup_w \partial B_w^m$, such that $\partial\Omega^m = \partial\Theta^m \cup \partial B^m$.

**JB:** *DONE: define aquifers with their z-coordinate, $z_m$ define the well $B_W$ at position $\boldsymbol{x}_W$ with radius $r_W$ as cylinder $\{|\boldsymbol{x} - \boldsymbol{x}_W| \leq \rho_W\}$. An finally $B_W^m = B_W \cap \Theta^m$.*

The distribution of the pressure head in $m$-th aquifer is described by Poisson equation and boundary conditions

$$\begin{aligned}
\nabla \cdot (-\mathbf{T}^m \nabla h^m) &= f^m \qquad \text{on } \Omega^m \subset \mathbf{R}^2,\ \forall m = 1, \ldots, M, && (1)\\
h^m|_{\Gamma_D^m} &= h_D^m, && (2)\\
(-\mathbf{T}^m \nabla h^m \cdot \boldsymbol{n})\,|_{\Gamma_N^m} &= 0, && (3)\\
(-\mathbf{T}^m \nabla h^m \cdot \boldsymbol{n})\,|_{\partial B_w^m} &= q_w^m \qquad \forall w \in \mathcal{W}, && (4)
\end{aligned}$$

where $\mathbf{T}^m$ [m$^2$s$^{-1}$] denotes the transmisivity tensor, $h^m$ [m] the pressure head, $f^m$ [ms$^{-1}$] source density, $\boldsymbol{n}$ unit normal vector on the boundary and $q_w^m = Q_w^m / |\partial B_w^m|$ is the density of the flow from the well to the aquifer over the well boundary $\partial B_w^m$. Equation (1) is derived from the Darcy law and the continuity equation for incompressible fluid.

Presuming the aquitards to be fully impermeable, the communication between aquifers is possible only through wells. We can prescribe the flow balance equation

$$\begin{aligned}
Q_w^m &= Q_{w,in}^m - Q_{w,out}^m, \text{ where} && (5)\\
Q_w^m &\ \ldots \text{ flow into aquifer across the well boundary,}\\
Q_{w,in}^m &\ \ldots \text{ flow from upper aquifer,}\\
Q_{w,out}^m &\ \ldots \text{ flow into lower aquifer.}
\end{aligned}$$

**PE:** *TODO: add arrow (flow) to the top*

Fig.1 presents the equation (5) and denotes the flows $Q_{w,\cdot}^m$ by red arrows. We can look at the flows in the balance equation as 1D problems which are governed by a difference of pressure heads and a transition coefficient. Using

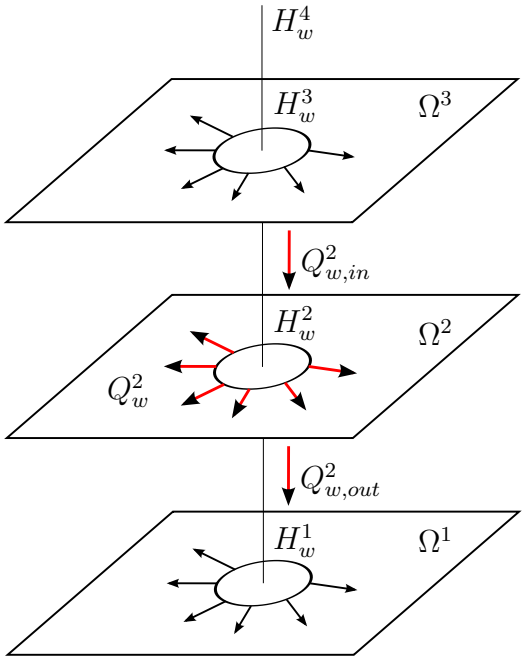


Figure 1: Flow balance in the well.

this idea, we can substitute the flows in the equation (5) and get

$$\int_{\partial B_w^m} \sigma_w^m \left(h^m - H_w^m\right) \, \mathrm{d}s = c_w^{m+1} \left(H_w^m - H_w^{m+1}\right) - c_w^m \left(H_w^{m-1} - H_w^m\right), \qquad (6)$$
$$\forall m = 1, \ldots, M \text{ and } \forall w \in \mathcal{W},$$

where $\sigma_w^m \, [\mathrm{ms}^{-1}]$ denotes the permeability coefficient between $w$-th well and $m$-th aquifer, $H_w^m$ the pressure head in the well $w$ at the level of $m$-th aquifer and finally $c_w^m \, [\mathrm{m}^2\mathrm{s}^{-1}]$ is the permeability of the well $w$ through aquitard $m$.

The problem is now to find set of functions $h^m \in C^2(\Omega^m) \cap C^1(\bar{\Omega}^m)$ and set of pressure values in the wells $H_w^m \in \mathbf{R}$, for all $m \in \{1, \ldots, M\}$ and $w \in \mathcal{W}$ that satisfy the equations (1) and (6).

Note that if the lower end of well is considered isolated from below, the coefficient must be set $c_w^1 = 0$. With $c_w^m = 0$ we can also simulate the end of the well $w$ at the level of aquifer $m$.

We mention yet the equation (6) for $m = M + 1$ which is one level above

the upmost aquifer and is adjusted to the form

$$c_w^M \left(H_w^M - H_w^{M+1}\right) = 0. \tag{7}$$

The pressure at the top of the well $H_w^{M+1}$ can be set as an input value or, if not set, is gained as part of the solution from the equation (7), see $H^4$ in Fig.1.

The boundary term in (6) with large $\sigma_w^m$ would force the pressure head along the well edge to be constant (equal $H_w^m$), which cannot be in general satisfied. Therefore it is weakened and later replaced by the average

$$\langle h^m \rangle = \frac{1}{|\partial B_w^m|} \int\limits_{\partial B_w^m} h^m \, \mathrm{d}s, \tag{8}$$

which corresponds to [1]. We use 200 points around the well edge for averaging but even smaller amount is possible since our test cases are symetric.

*2.1. Weak formulation*

We define the trial and the test spaces

$$V = \prod_{m=1}^{M} \left(H^1(\Omega^m) \times \mathbf{R}^W\right), \tag{9}$$

$$V_0 = \prod_{m=1}^{M} \left(H_0^1(\Omega^m) \times \mathbf{R}^W\right), \tag{10}$$

where $H^1$ and $H_0^1$ are standard Sobolev spaces and

$$H_0^1(\Omega^m) = \{\varphi \in H^1(\Omega^m); \varphi|_{\Gamma_D^m} = 0\}.$$

We can now introduce the weak solution $u$ and test functions $v$

$$u = (h^1, \ldots, h^M, H_1^1, \ldots, H_W^{M+1}) \in V, \tag{11}$$

$$v = (\varphi^1, \ldots, \varphi^M, \Phi_1^1, \ldots, \Phi_W^{M+1}) \in V_0. \tag{12}$$

To obtain the weak form we apply the standard Galerkin method. We multiply the equations (1) by test functions $\varphi^m$ and integrate by parts over $\Omega^m$, for all $m = 1, \ldots, M$, to get

$$\int\limits_{\Omega^m} T^m \nabla h^m \cdot \nabla \varphi^m \, \mathrm{d}\boldsymbol{x} + \sum_{w \in \mathcal{W}} \int\limits_{B_w^m} \sigma_w^m (h^m - H_w^m) \varphi^m \, \mathrm{d}\boldsymbol{x} = \int\limits_{\Omega^m} f^m \varphi^m \tag{13}$$

We then multiply (6) by $\Phi_w^m$, subtract it from (13) and use (8) which results in

$$\int_{\Omega^m} T^m \nabla h^m \cdot \nabla \varphi^m \, \mathrm{d}\boldsymbol{x} + \sum_{w \in \mathcal{W}} \sigma_w^m \left( \langle h^m \rangle - H_w^m \right) \left( \langle \varphi^m \rangle - \Phi_w^m \right) + \\ + \sum_{w \in \mathcal{W}} \left[ c_w^{m+1} \left( H_w^m - H_w^{m+1} \right) \Phi_w^m - c_w^m \left( H_w^{m-1} - H_w^m \right) \Phi_w^m \right] = \\ = \int_{\Omega^m} f^m \varphi^m \, \mathrm{d}\boldsymbol{x} \quad \forall m = 1, \ldots, M. \quad (14)$$

**JB:** *Consider sum over aquifers to get square term from communication on wells. Boundary conditions on wells?*

## 3. Discretization

We can now proceed to the choice of the enrichment and discretize the system of equations (14). Let's imagine that we have only one aquifer so we can omit the upper index $m$ in this section. In fact, it is appropriate to do so in some notations of shape functions because we do consider the same triangulation for every aquifer in our implementation.

### *3.1. Enrichment function*

The enrichment function in general can be obtained from the knowledge of the solution character or from the solution of a simple local problem which will provide us the function. In our case the simple problem is finding pressure distribution in a circular domain $\Omega$ with one well placed at the center. It can be easily proved that the function

$$h = a \log(r_w) + b, \quad (15)$$

where $r_w$ is a distance function

$$r_w(\boldsymbol{x}) = \|\boldsymbol{x} - \boldsymbol{x}_w\| = \sqrt{(x - x_w)^2 + (y - y_w)^2}, \quad (16)$$

is the solution of a Laplace equation $-T\Delta h = 0$, just by putting the function into the equation. **JB:** *DONE:Rather move close to the definition of enrichment function.* We see in (15) the logarithmic dependence of the pressure head on the distance from the well. If we represented the well only by a point,

the pressure head would go to infinity while closing to the point (singularity $\lim_{r\to 0} \log r = -\infty$). Instead, we keep in mind the radius of the well $\rho_w$ and introduce (global) enrichment function **JB:** *DONE: Change notation R for enrichment radius, $\rho_W$ for radius of the well.*

$$s_w(\boldsymbol{x}) = \begin{cases} \log(r_w(\boldsymbol{x})), & r_w > \rho_w \\ \log(\rho_w), & r_w \leq \rho_w \end{cases}. \tag{17}$$

See Fig.2. It is natural to use the same set of $s_w$ on each aquifer since they depends only on $r_w$ and the wells are placed at the same positions throughout the aquifers (we consider only vertical wells, perpendicular to aquifers).

**PE:** *DONE: do not forget to replace the notation of the enrichment function*

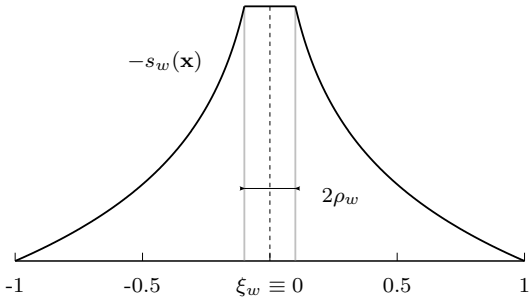


Figure 2: The enrichment function.

**PE:** *DONE: define enrichment zone*

In contrast to global enrichment methods, XFEM and SGFEM apply the enrichment functions only locally. The area of the enrichment in our case is a circle of radius $R$ around a well. $R$ will be further called the enrichment radius.

### *3.2. Partition of unity methods*

Let $N_\alpha(\boldsymbol{x})$, $\alpha \in \mathcal{I} = \{1, \ldots, N\}$ be the standard linear finite element shape functions associated with the node $\boldsymbol{x}_\alpha$ of the triangulation. In **standard XFEM**, we write the solution in the form

$$h(\boldsymbol{x}) = \sum_{\alpha\in\mathcal{I}} a_\alpha N_\alpha(\boldsymbol{x}) + \sum_{w\in\mathcal{W}} \sum_{\alpha\in\mathcal{I}_w^e} b_{\alpha w}\phi_{\alpha w}(\boldsymbol{x}), \tag{18}$$

where $a_\alpha$ are the standard FE degrees of freedom and $b_{\alpha w}$ are degrees of freedom coming from enrichment of the well $w$. The index set $\mathcal{I}_w^e$ includes all nodes enriched by the well $w$, which means that we have several enrichment functions and each can enrich different nodes. The local enrichment functions $\phi_{\alpha w}$ in (18) are defined in the following way

$$\phi_{\alpha w} = N_\alpha(\boldsymbol{x}) L_{\alpha w}(\boldsymbol{x}), \quad \alpha \in \mathcal{I}_w^e, w \in \mathcal{W}, \tag{19}$$

where simply the enrichment function $L_{\alpha w}(\boldsymbol{x}) = s_w(\boldsymbol{x})$. **PE:** *TODO: define test functions, refer to the weak form*

*3.2.1. Corrected XFEM*

The corrected XFEM [3] deals with the convergence problem on blending elements and introduces the **ramp function**

$$\begin{aligned} G_w(\boldsymbol{x}) &= \sum_{\alpha \in \mathcal{I}_w^e} N_\alpha(\boldsymbol{x}) \\ &= \begin{cases} 0 & \text{on unenriched elements} \\ 1 & \text{on elements where all nodes are enriched} \\ ramp & \text{on elements where some of the nodes are enriched} \end{cases} \end{aligned} \tag{20}$$

It also extends the set of enriched nodes, denoted by $\mathcal{J}^e$, by enriching (unenriched) nodes on elements, where only some of the nodes are in $\mathcal{I}^e$. Thus $\mathcal{I}^e \subset \mathcal{J}^e$ and there are more enriched nodes. The enrichment function changes into the form

$$L_{\alpha w} = G_w(\boldsymbol{x}) s_w(\boldsymbol{x}), \quad \alpha \in \mathcal{J}^e, w \in \mathcal{W}. \tag{21}$$

**JB:** *DONE: Who are they? introduce shifed XFEM method and giv the same reference.* In [3], they further suggest the **shifted** enrichment functions in order to preserve the property of standard FE approximation at nodes $h(\boldsymbol{x}_\alpha) = a_\alpha$; the value at the node is equal the corresponding degree of freedom. The enrichment functions must be then zero at the nodes which is satisfied in the form

$$L_{\alpha w} = G_w(\boldsymbol{x}) \left[ s_w(\boldsymbol{x}) - s_w(\boldsymbol{x}_\alpha) \right], \quad \alpha \in \mathcal{J}^e, w \in \mathcal{W}. \tag{22}$$

The property of the shifted formulation enables us to prescribe Dirichlet boundary condition such that $a_\alpha = h_D(\boldsymbol{x}_\alpha)$.

For the purpose of this article, let's call the two methods described above the **ramp function XFEM** and the **shifted XFEM**, as we shall reference to them later. **JB:** *DONE: I prefer to be more explicit and use "ramp function XFEM" and "shifted XFEM", this is more clear for a reader familiar with the topic.*

*3.2.2. SGFEM*

Finally we present the **SGFEM**, according to [4, 5]. The enrichment function is defined as the subtraction of the global enrichment function and its interpolation

$$L_{\alpha w} = \left[ s_w(\boldsymbol{x}) - \pi_\tau(s_w)(\boldsymbol{x}) \right], \qquad \text{on } \tau,\ \alpha \in \mathcal{I}^e, w \in \mathcal{W}. \tag{23}$$

where the interpolation $\pi_\tau$ is built using the finite element shape functions associated with nodes $\mathcal{I}(\tau)$ of the element $\tau$

$$\pi_\tau(s_w)(\boldsymbol{x}) = \sum_{\beta \in \mathcal{I}(\tau)} s_w(\boldsymbol{x}_\beta) N_\beta(\boldsymbol{x}). \tag{24}$$

Of course $\alpha \in \mathcal{I}(\tau)$ in (23). Notice that there are no additional enriched nodes on blending elements, like in $\mathcal{J}^e$ in (21) and (22), and no ramp function is involved.

**JB:** *I miss explicit specification of discrete spaces.*

## 4. Test problems

In this section we define problems that we solve in our numerical experiments. We restrict ourselves to single aquifer problems for the purpose of this article but our implementation enables multi-aquifer systems as well. In order to measure convergence it is desirable to have an analytic solution which is available in the two following cases.

**Problem 1 (Laplace equation).** Find the solution $h$ of a single aquifer problem

$$\begin{aligned} -T\Delta h &= 0 \qquad \text{on } \Omega \\ h|_{\partial\Omega} &= h_D \\ h|_{B_w} &= P_w \\ (-T\nabla h \cdot \boldsymbol{n})\,|_{\partial B_w} &= q_w \end{aligned}$$

where the pressure $P_w$ at the well edge $B_w$ and the pressure $h_D$ at the boundary are given. The domain $\Omega$ is a square with a single well placed near the center in $\boldsymbol{x}_w$.

We can find the analytic solution of Problem 1 but on a circular disk where we have the constant pressure $P_D$ on the outer boundary. Let us remind the function $h = a\log(r_w) + b$ (which we used in (15) to define the enrichment function) and use the boundary conditions to find the constants $a, b$ such that they satisfy

$$\begin{aligned} a\log(\rho_w) + b &= P_w, \\ a\log(R) + b &= P_D, \end{aligned}$$

where $R$ is the radius of the circular domain and $\rho_w$ is the well radius. The solution is then

$$h = a\log(r_w) + b \qquad \text{with } a = \frac{P_w}{\log\left(\frac{\rho_w}{R}\right)},\ b = -a\log R \tag{25}$$

The function (25) is just the analytic solution of Problem 1 when (25) is used to compute $h_D$ on the square boundary, with $R$ being the half diagonal of the square.

**Problem 2 (Poisson equation).** Find the solution $h$ of a single aquifer problem with a source term

$$\begin{aligned} -T\Delta h &= TU\omega^2\sin(\omega x) \qquad \text{on } \Omega \\ h|_{\partial\Omega} &= h_D + U\sin(\omega x) \\ h|_{B_w} &= P_w \\ (-T\nabla h\cdot\boldsymbol{n})\,|_{\partial B_w} &= q_w \end{aligned}$$

where $U$ and $\omega$ are given.

The analytic solution of Problem 2

$$h = a\log(r_w) + b + U\sin(\omega x), \tag{26}$$

is obtained the same way as above, with $a, b$ from (25).

The input parameters for the numerical tests of Problem 1 and Problem 2 are gathered in the table 1.

| parameter | value |
|---|---|
| $\Omega$ | $(-100, 100) \times (-100, 100)$ |
| $\boldsymbol{x}_w$ | $[5.43, 5.43]$ |
| transimisivity $T$ | 1.0 |
| boundary pressure $P_D$ | 0.0 |
| well pressure $P_w$ | 100.0 |
| well radius $\rho_w$ | 0.2 |
| $\sigma_w$ | $10^5$ |
| $c_w^0$, $c_w^1$ | 0.0, $10^{13}$ |
| $U$ | 0.03 |
| $\omega$ | 8.0 |

Table 1: Input parameters for the numerical tests. Units are omitted. **PE:** *TODO: Are the units necessary here?*

## 5. Integration on enriched elements

In order to compute the entries of the system matrix, we need to integrate the expressions containing the enrichment functions. These of course can be non-polynomial, like they are in our case. The standard quadrature rules are not appropriate any more, as they are constructed to integrate precisely polynomials up to a given degree. The higher requirements on integration precision are the price for using enrichment functions and a coarse mesh.

There are two aspects which the integration must handle properly:

- the steep gradient of enrichment base functions in the vicinity of a well (the singularity), **JB:** *DONE: in fact it is the steep gradiant of enrichment base functions.*
- the well edge (since the elements of the triangulation do not take the well into account)

Since the integrated functions can be very large near the singularity, even small changes in the domain shape can lead to large errors in integration.

**JB:** *DONE: Should mention that due to the singularity the integrated function is very large and small changes in the domain shape can lead to big erros.*

One of the approaches to improve integration is an adaptive quadrature. This way we divide the element into small pieces (squares) only to place more quadrature points inside but not to bring any more degrees of freedom in the system. We will discuss the adaptivity criteria, suggest improvement and compare our solution with the original one in this subsection. We will refer also some of the convergence results which will be shown later in 9.

### *5.1. Adaptive refinement of an element*

**JB:** *Rather use term "adaptive quadrature" then local element refinement. Finite elements remain untouched.*

Gracie and Craig used in [1] a criterion for adaptive refinement according to which only the subelements that have nonzero cross-section with the well are refined. This catches nicely the well edge but it can work well only in some special cases when the well is at the node of an element or near the center of an element. The problem comes when the well is placed near the edge or node of an element. In that case there can be large difference in the size of neighboring subelements as you can see in Fig.3a. Although the integrand is computed precisely enough on the element with the well inside, the quadrature points on the neighboring elements (where the pressure head gradient can be still large) are placed very sparsely and the integration error is large.

We suggested additional criterion for subelements refinement which takes into account a subelement diameter and its distance from the well

$$d_T > C_R |d_{min} - \rho_w|, \tag{27}$$

where $d_T$ is the diameter of the subelement and $d_{min}$ is minimal distance between a vertex of the subelement and the well edge. $C_R$ is a scaling constant, equal 1.0 by default, through which we can control the significance of the criterion.

In this way, the elements in which the well does not lie are also refined as you can see in Fig.3b. The quadrature points are then distributed more 'smoothly' around the well and the integrals with gradients can be computed more accurately.

In Fig.4 you can see the $L_2$ norms of the error on the enriched elements which were computed also using the corresponding adaptive integration. Notice the scale of the improved version – the error on elements is in small range and is not significantly concentrated anywhere. On the other hand,

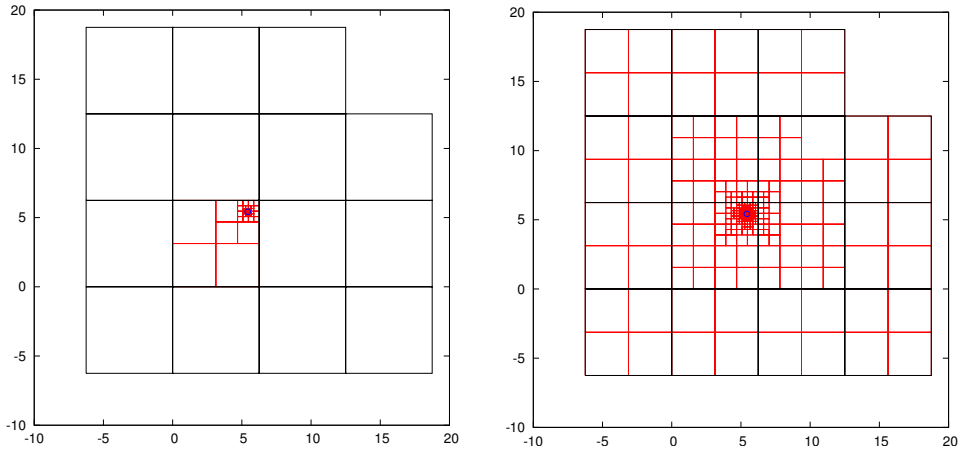


(a) original refinement (b) improved refinement

Figure 3: Comparison of the original and improved refinement techniques. Black lines denote enriched element edges, red lines denote adaptive refinement (subelement edges) and the well edge is blue.

the original version shows out large error that is concentrated on the closest non-refined element to the well.

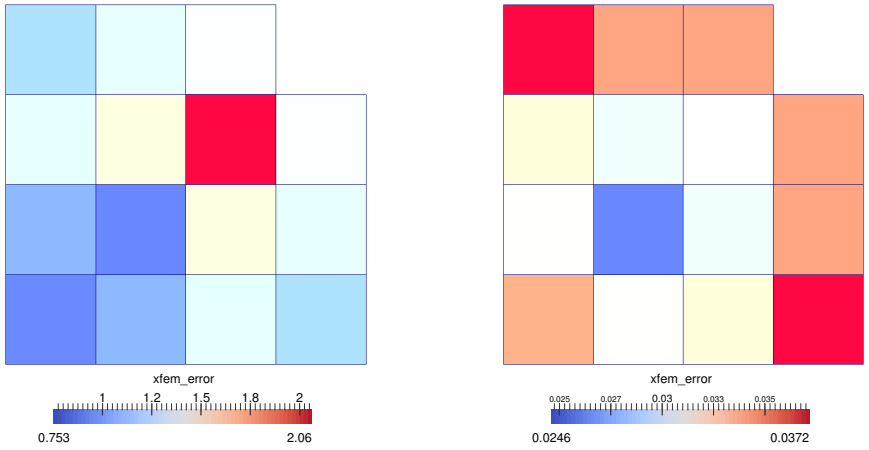


(a) original refinement (b) improved refinement

Figure 4: Comparison of element-wise error in $L_2$ norm using different refinement techniques.

**PE:** ** non-optimal convergence rate with the approach of [gracie] and their integration scheme 3-4*
** the above can be improved by using higher order quadrature rules (6-6)*
** problem is that we do not represent the well edge and mainly its surrounding well enough*

## 6. A priori adaptive quadrature

Let us assume just one well of radius $\rho$ situated at the origin. The worst term to integrate is

$$f(r) = (\nabla \log r)^2 \approx r^{-2} \tag{28}$$

independently of the particular variant of the PUM method. Consider a square $S$ with a side $h$ and let us denote $r_{min}$ and $r_{max}$ the minimum and maximum distance to the origin respectively. We shall estimate the error of the 2D tensor product Gauss quadrature rule of the order $n$ on the square $S$ by the error of 1D quadrature of the same order on $(r_{min}, r_{min} + h)$:

$$E^n(S) \leq hE^n((r_{min}, r_{min} + h)).$$

This is a conservative estimate, which is natural for elements near the main $x$ and $y$ axis, where the error is maximal.

To guarantee prescribed tolerance $\epsilon$, we want to control the error density

$$E^n(S)h^{-2} \leq h^{-1}E^n((r_{min}, r_{min} + h)) \leq \epsilon. \tag{29}$$

Formula for the error of 1D Gauss quadrature of order $n$ ($n$ quadrature points). Quadrature error for $\int_r^{r+h} f$ is

$$E_n = \frac{h^{2n+1}(n!)^4}{(2n+1)((2n)!)^3} f^{(2n)}(\xi_n)$$

for some $\xi_n \in (r, r + h)$. For the term of interest, i.e. (28), we have

$$|f^{(2n)}(r)| = (2n + 2)!r^{-(2n+2)},$$

then the convergence criterion following from (29) reads:

$$h^{-1}E_n = \alpha_n \left(\frac{h}{r_{min}}\right)^{2n} \frac{1}{r_{min}^2} \leq \epsilon, \qquad \alpha_n = (2n + 2) \left(\frac{(n!)^2}{(2n)!}\right)^2$$

Derived criterion holds only on squares, where the integrated function is smooth. This is not the case for squares intersecting the boundary of the well, $r_{min} \leq \rho \leq r_{max}$, where we integrate discontinuous function $\chi_{S \setminus W} f$. Using substitution, we can map $W$ to unit circle $B$

$$\int_S \chi_{S \setminus W} \frac{1}{r^2} \mathrm{d}\boldsymbol{r} = \int_{S'} \chi_{S' \setminus B} \frac{1}{r'^2} \mathrm{d}\boldsymbol{r'},$$

where $S'$ is square with side $H = h/\rho$ and $\boldsymbol{r'} = \boldsymbol{r}/\rho$. Empiricaly determined error of the midpoint rule for later integral is

$$E(H) = c_e H^{p_e}, \quad \text{with } c_e = 0.08,\ p_e = 2.5.$$

This error has to be smaller then $\epsilon h^2$, thus for $h$ we get formula:

$$h \leq h_b(\epsilon) = \left( \frac{\epsilon \rho^{p_e}}{c_e} \right)^{\frac{1}{p_e - 2}}. \tag{30}$$

Based on the presented analysis above, we propose following rules for adaptive quadrature:

1. If $r_{max} < \rho$ the square quadrature is zero.
2. If $r_{min} < \rho < r_{max}$. For $h \geq h_b(\epsilon)$ subdivide the square, else use lowest order quadrature for original function (i.e. $f(r) = 0$ for $r \leq \rho$).
3. If $r_{min} > \rho$. For $\frac{h}{r_{min}} > \frac{1}{2}$ subdivide the square, else select order $n$ so that
$$\frac{\alpha_n h^{2n}}{r_{min}^{2n+2}} \leq \epsilon, \tag{31}$$
use at least the same order as necessary for FEM.

**JB:** *TODO: We should estimate true error numericaly using one more subdivision and compare it to prescribed tolerance, we should be safely below, without increasing the number of evaluation comapred to current implementation.*

### *6.1. Adaptive integration experiment*

We now describe the experiment from which we obtained the coefficients in the criterion (30). Let us have a single element, a square $4 \times 4$, out of which a circle of unit radius is cut off – this represents an element with a well. We now want to investigate integration error in the vicinity of the circle on the function $f = r^{-2}$, $r$ being the distance from the center of the circle.

We compute the integral on the selected level of refinement only on the squares intersecting the circle. Then we refine the squares up to the 12-th level, integrate again and compute the difference. Quadratures rules $1 \times 1$, $2 \times 2$, $3 \times 3$ and $4 \times 4$ are used. The results are shown in Fig.5 also with convergence trend lines equations. The conclusion can be made that it is more efficient to refine one more level with one-point quadrature than to use higher order quadrature on the coarser level. As for the coeffiecient, these can be read from the graph – for the one point quadrature $c_e = 12.65$ and $p_e = 1.27$.

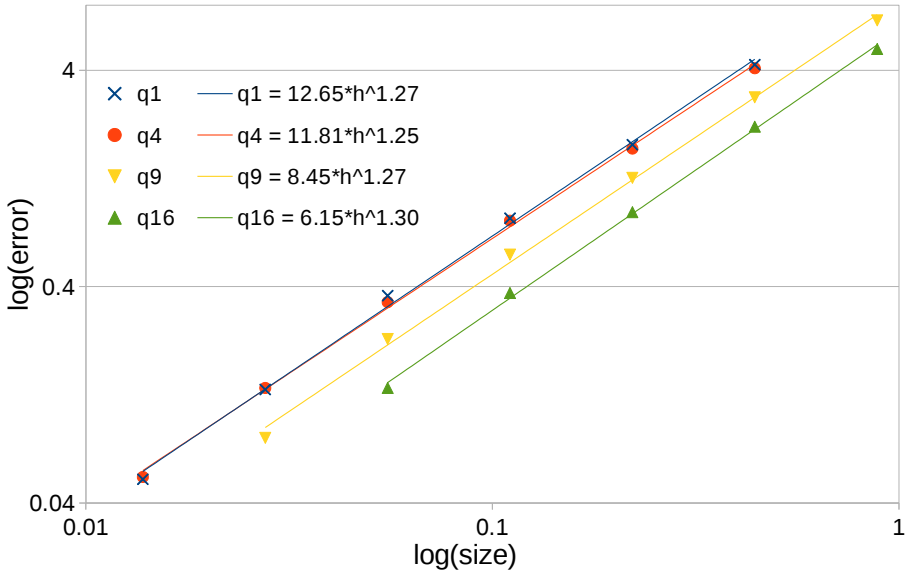


Figure 5: Convergence graph of adaptive quadrature on function $r^{-2}$.
**PE:** *thicker trend lines*

## 7. Estimate the enrichment radius

The enrichment is done in order to diminish approximation error of the precise solution of the problem, i.e. $\tilde{e}_h = \inf_{u_h \in V_h} \|u - u_h\|_V$. Let us consider a single well at the origin. The solution can be splitted $u = u_s + u_r$ to the singular part $u_s(\boldsymbol{x}) = \log|\boldsymbol{x}|$ and the regular part $u_r = u - u_s$. Using

standard error estimate for eliptic PDE (see e.g. [7]) we get

$$\begin{aligned}\|u-u_h\|_{H^1(\Omega)} &\le c_a \inf_{u_h\in V_h^P}\|u-u_h\|_{H^1(\Omega)}\\ &\le c_a\big(\inf_{u_h\in V_h}\|u_s-u_h\|_{H^1(\Omega)}+\inf_{u_h\in V_h^P}\|\log|\boldsymbol{x}|-u_h\|\big)_{H^1(\Omega)} \qquad (32)\end{aligned}$$

state with a radius $R$ of the enrichment should be chosen so that

$$\min_{u_h\in V_h^P}\|\log\boldsymbol{x}-u_h\|_{V(\Omega^P)}\le\epsilon$$

where $V_h^P$ is polynomial finite element approximation space on unenriched part $\Omega^P$ of the domain $\Omega$, $V=H^1(\Omega)$, and $\epsilon$ is prescribed tolerance.

For linear elements and 1D case, we get

$$\begin{aligned}\|\log x-u_h\|^2_{L^2(r,r+h)} &= h\int_0^1|\log(r+ht)-\big[(1-t)\log r+t\log(r+h)\big]|^2\mathrm{d}t\\ &= \frac{h^5}{4r^4}\int_0^1 t^2(1-t)^2+O(h^6)\approx\frac{h^5}{120r^4}\end{aligned}$$

$$\begin{aligned}\|\nabla(\log x-u_h)\|^2_{L^2(r,r+h)} &= h\int_0^1|\frac{1}{r+ht}-\frac{\log(r+h)-\log r}{h}|^2\mathrm{d}t\\ &= \frac{h^3}{r^4}\int_0^1(\frac{1}{2}-t)^2+O(h^4)\approx\frac{h^3}{12r^4}\end{aligned}$$

And thus,

$$\|\log x-u_h\|_{H^1(r,r+h)}\approx h^{3/2}r^{-2}12^{-1/2}. \qquad (33)$$

We confirm the validity of the estimate (33) in 2D case by a numerical test. The ratio

$$\frac{h^{3/2}r^{-2}12^{-1/2}}{\|\log\boldsymbol{x}-u_h\|^2_{H^1(T)}} \qquad (34)$$

is computed on every element $T$ of the mesh using a $5\times5$ Gaussian quadrature, with $h$ being the element diameter and $r$ being the distance between the element center and the origin. The results on five refined meshes are gathered in the table 2. We can see from the 'min' column of the table 2 that the ratio is very close to 1.0 which means we have a good upper estimate. The value in brackets at the finest refinement pertains to several elements

| $h$ | | min | max |
|---|---|---|---|
| $^{14}/_{8}$ | | 0.97 | 7.1 |
| $^{14}/_{16}$ | | 0.99 | 16.4 |
| $^{14}/_{32}$ | | 1.00 | 34.4 |
| $^{14}/_{64}$ | | 1.00 | 70.3 |
| $^{14}/_{128}$ | (0.756) | 1.00 | 142.0 |

Table 2: Numerical validation of the estimate (33) in 2D case. The minimal and maximal values of (34) are collected in the table for different refinements. **PE:** *DONE: Seems that there is still a coeffient close to* $\sqrt{2}$.

near the well where the used quadrature is too coarse. However the ratio is greater than or equal 1.0 elsewhere.

Further we can see the error in $H^1$ norm over the elements in the Fig.6a. We can compare it with the ratio in the Fig.6b and see that the ratio iis closest to 1.0 (our estimate is best) where the error is largest (in $x$ and $y$ directions) and otherwise in diagonal directions. We can also notice that the logarithm is better approximated by the linear functions in the diagonal directions than in the axes directions.

Let us consider a 2D domain. The $H^1$ error on elements in distance $r$ is same as in the 1D case up to a constant close to 1 as we have seen above. Thus error on the band at distance $r$ is proportional to

$$\| \log \boldsymbol{x} - u_h \|^2_{H^1(\Omega^P)} \approx \int_R^{diam\Omega} 2\pi r \frac{h^3}{12r^4} \mathrm{d}r \leq \frac{2\pi h^3}{12} \frac{1}{2R^2} \approx \frac{h^3}{4R^2}. \tag{35}$$

Then, the optimal choice of $R$ for given $H^1$ tolerance $\epsilon$ follows directly from (35)

$$R = \frac{h^{3/2}}{4\epsilon} \tag{36}$$

We demonstrate the behaviour of the model depending on the enrichment radius choice on our test case with source term present. **PE:** *Define the two test case - with and without source.* The convergence graph in Fig.7 shows how the error depends on the element size for different enrichment radius. As a reference in the graph, we added the error of classical FEM applied on the same problem but with well omitted – the convergence rate is optimal

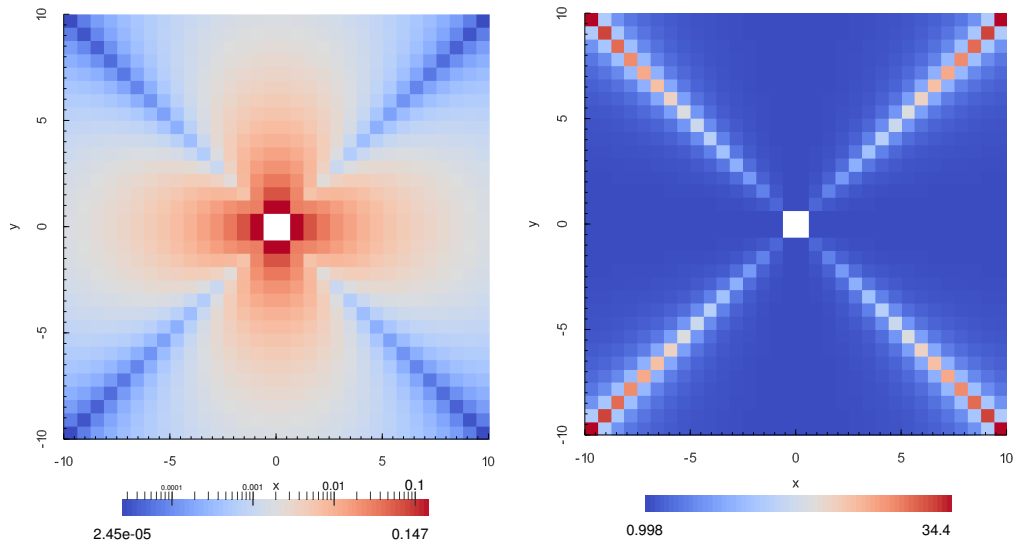


(a) $\| \log \boldsymbol{x} - u_h \|^2_{H^1(T)}$ in log scale (b) the ratio (34)

Figure 6: **PE:** *Exchange figures with correct scales – after running corrected test.* Results of the numerical validation of the estimate (33). The elements are left out in the center where the log singularity is situated and where the function is cut off.

2.0. We see that the convergence rate for all the chosen enrichment radii is very close to the optimum. It is degraded for smaller element size while we are approaching the accuracy limits of the integration.

We also see in Fig.7 that the error is not decreasing significantly for larger enrichment radii. This trend is more obvious from the graph in Fig.8 which shows the dependance of the error on the enrichment radius for different element sizes.

## 8. Condition number

Condition number for matrices resulting from conforming FEM applied to Laplace equation is $O(h^{-2})$, so the iteration count for CG without preconditioning is $O(h^{-1}) = O(\sqrt(n))$, where $n = 1/h^2$ is number of DOFs. With local preconditioning (Jacobi, SOR, ILU) one can usually achieve number of iteration $O(h^{-0.5})$, c.f. [8].

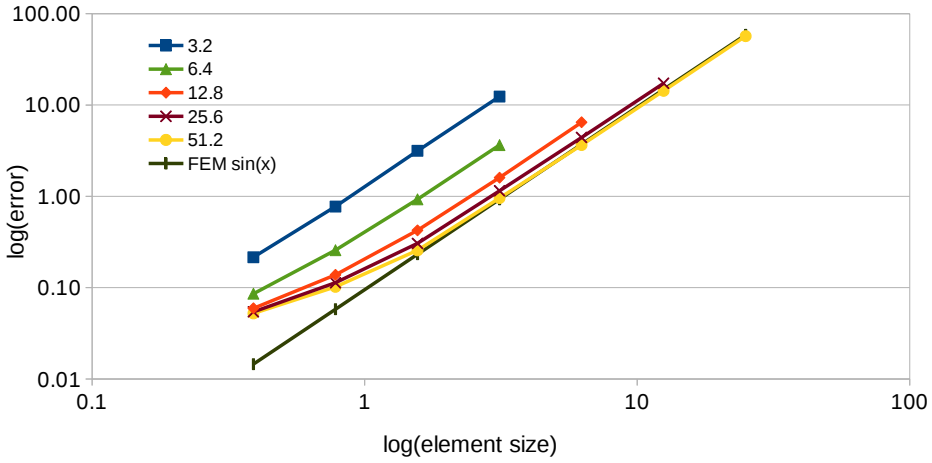


Figure 7: Convergence graph for different enrichment radii. The 'FEM sin(x)' data comes from the problem without well solved by classical FEM and with optimal convergence rate 2.0.

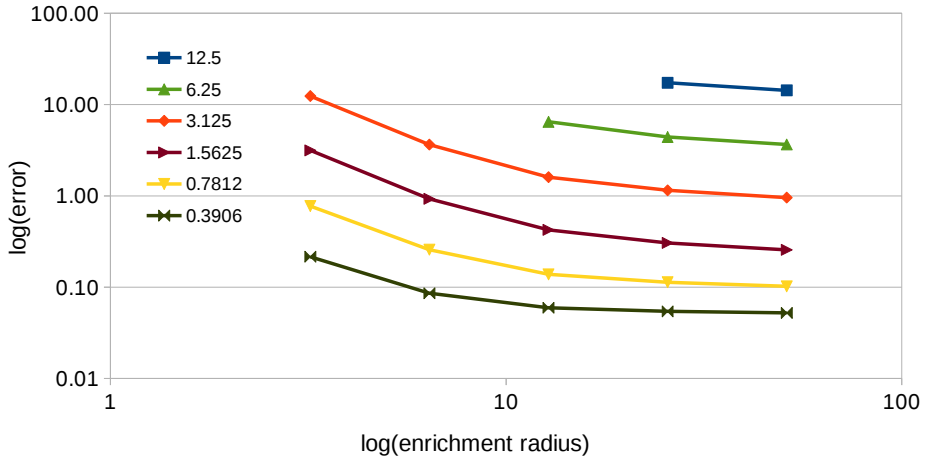


Figure 8: Dependence of the error on the enrichment radius for different element sizes.

## 9. Results

In this section we present the main results. We solve Problem 1 and Problem 2 defined in section 4 with the methods described in 3.2 and compare them.

Let us start with the Problem 1 and look at the convergence graph in Fig.9. At first we solve the problem by standard FEM with adaptive mesh refinement where 30% of the elements with the highest error estimate are refined (the element size is then taken at the smallest elements in the vicinity of the well). We see that the convergence is slow until the size of elements reaches the scale of the well. Therefore we divided the graph in two parts with convergence rates 0.56 and 1.27.

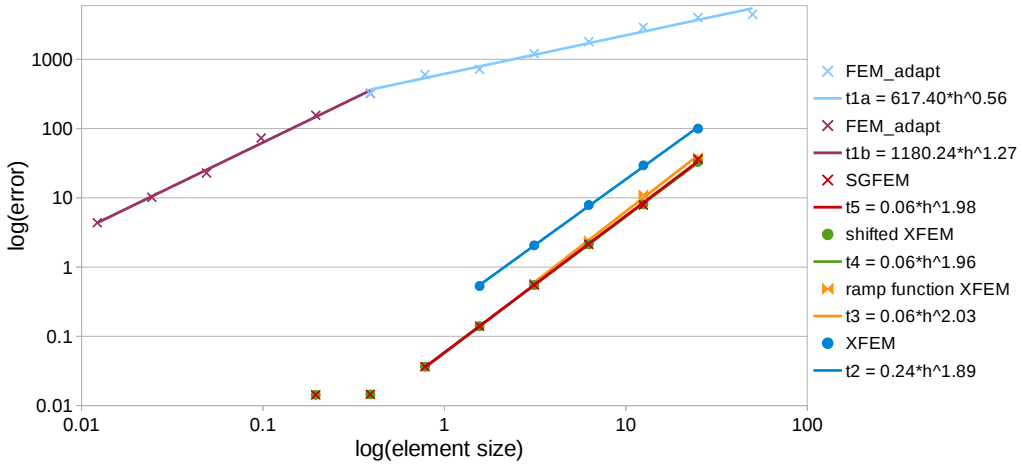


Figure 9: Convergence graph of different methods on Problem 1.

## 10. Summary

## 11. Acknowledgement

This work was made under the sincere guidance and support of Mgr. Jan Březina, Ph.D.

This work was supported by the Ministry of Education of the Czech Republic within the SGS project no. 21066/115 on the Technical University of Liberec.

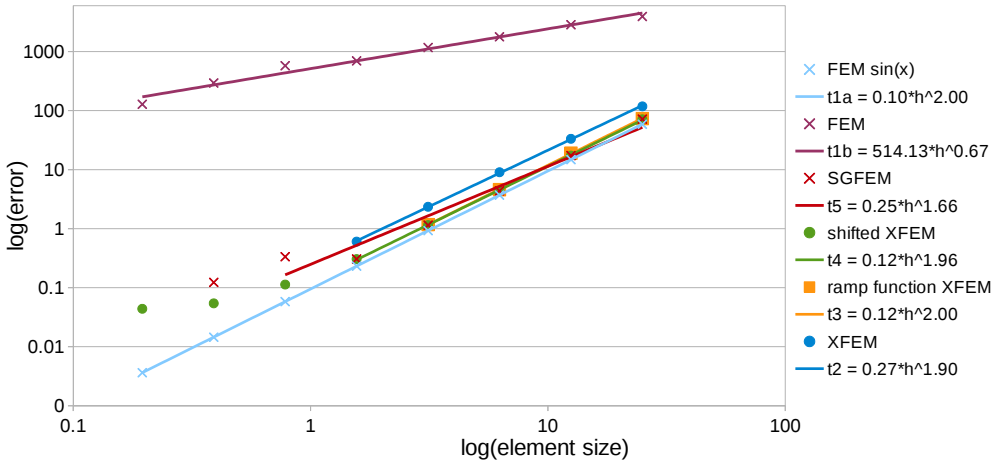


Figure 10: Convergence graph of different methods on Problem 2. The 'FEM sin(x)' data comes from the problem without well solved by classical FEM and with optimal convergence rate 2.0.


[1] R. Gracie, J. R. Craig, Modelling well leakage in multilayer aquifer systems using the extended finite element method, Finite elements in Analysis and Design, Elsevier B.V. 46 (2010) 504–513.

[2] J. R. Craig, R. Gracie, Using the extended finite element method for simulation of transient well leakage in multilayer aquifers, Advances in Water Recources, Elsevier B.V. 34 (2011) 1207–1214.

[3] T. P. Fries, A corrected XFEM approximation without problems in blending elements, International Journal for Numerical Methods in Engineering 75 (2007) 503–532.

[4] I. Babuška, U. Banerjee, Stable Generalized Finite Element Method (SGFEM), Computer Methods in Applied Mechanics and Engineering 201 (2012) 91–111. arXiv:1104.0960.

[5] V. Gupta, C. A. Duarte, I. Babuška, U. Banerjee, A stable and optimally convergent generalized FEM (SGFEM) for linear elastic fracture mechanics, Computer Methods in Applied Mechanics and Engineering 266 (2013) 23–39.

[6] W. Bangerth, R. Hartmann, G. Kanschat, deal.II – a general purpose object oriented finite element library, ACM Trans. Math. Softw. 33 (4) (2007) 24/1–24/27.

[7] D. N. Arnold, Lecture notes on Numerical Analysis of Partial Differential Equations, 2009.
URL http://www.ima.umn.edu/~arnold//8445.f11/notes.pdf

[8] A. Ern, J.-L. Guermond, Evaluation of the condition number in linear systems arising in finite element approximations 40 (1) 29–48. doi:10.1051/m2an:2006006.